SAND2014-0592J

Theoretical and experimental quantification of doubly and singly differential cross sections for electron-induced ionization of isolated tetrahydrofuran molecules

C. Champion[1], M. A. Quinto[1], M. U. Bug[2], W. Y. Baek[2] and P. F. Weck[3]

[1]*Université Bordeaux 1, CNRS/IN2P3, Centre d'Etudes Nucléaires de Bordeaux-Gradignan, CENBG, France*

[2]*Physikalisch-Technische Bundesanstalt PTB, Braunschweig, Germany*

[3]*Sandia National Laboratories, Albuquerque, NM, USA*

Abstract:

Electron-induced ionization of the commonly used surrogate of the DNA sugar-phosphate backbone, namely, the tetrahydrofuran molecule, is here theoretically described within the 1st Born approximation by means of quantum-mechanical approach. Comparisons between theory and recent experiments are reported in terms of doubly and singly differential cross sections.

Keywords: ionization, cross sections, electron impact, tetrahydrofuran molecule

Corresponding author:

Electronic mail: champion@cenbg.in2p3.fr

Université Bordeaux 1, CNRS/IN2P3, Centre d'Etudes Nucléaires de Bordeaux-Gradignan, CENBG, Chemin du solarium, BP 120, 33175 Gradignan, France

1. Introduction

Irradiations of biological matter by charged particle beams produces many secondary species along the projectile track that can further react within irradiated cells and then provoke complex cellular damages, among which the double strand breaks are nowadays clearly identified as the most important ones since leading to a profound modification of the genetic material and therefore, in some cases, to the cellular death. In this context, investigating the interactions induced by ionizing particles on DNA components is of fundamental importance in many multi-disciplinary scientific fields like radiobiology, radioprotection but also medicine including radiotherapy and nuclear imaging. However, the dedicated literature remains limited to a low number of studies. This lack - of both experimental and theoretical data - becomes even critical in radiobiology where modeling the charged particle histories in biological matter undoubtedly requires an accurate set of input data, namely, the collision cross sections, for describing the radiation-induced damages at the sub-cellular level. In fact, this limitation is usually overcome by means of an artifice, which consists in using the water molecule as surrogate of the living material, this latter being the major component of human body, amounting to about 60-80% in mass.

On the experimental side, until recently, measurements on biological systems have been restricted to studies of the mechanisms of the radiation damage only explored at the mesoscopic scale and not at the single molecule, nanometric, scale. Thus, except for the elastic scattering process - which has been extensively investigated by many groups (see for example Ref.[1]) - the ionization and therefore the fragmentation of isolated gas-phase DNA components have received only little interest. Furthermore, let us add that the experiments remain - in the major part - essentially focused on total cross section measurements, the multiple differential cross sections being obviously more complex, mainly due to the difficult task of resolving the different target molecular orbitals, which may be very closely spaced in energy (~1 eV). Moreover, when they exist, the experimental studies essentially report on *relative* cross sections and then do not permit

to check the existing theories. In this context, let us cite the work of Colyer et al. [2] dedicated to dynamical multi differential studies on the tetrahydrofuran (THF) molecule commonly seen as a simple model for the deoxyribose building block of DNA - and that of Builth-Williams et al. [3] where triply differential cross sections are reported for pyrimidine ($C_4H_4N_2$) molecules. Similarly, Bellm et al. [4] have recently reported triply differential cross sections for the electron-impact ionization of inner valence orbitals of thymine induced by 250 eV incident electrons. As highlighted above, total cross sections of positive- and negative-ion production on bio-molecular targets are more abundant in the literature. Let us cite the measurements of ionic fragments of THF performed by Fuss et al. [5] and those more recently obtained by Dampc et al. [6] on the absolute and relative scale, respectively. In this context, we refer the interested reader to the absolute total cross section measurements reported by Możejko et al. [7] and more recently by Baek et al. [8] for a tetrahydrofuran target as well as those reported by Shafranyosh and coworkers [9-11] for cytosine and thymine molecules. Finally, let us also mention the works on RNA-uracil nucleobase ionization provided by Feil et al. [12] where relative total cross sections were reported for uracil molecules impacted by electron with energies ranging from the ionization threshold up to1 keV.

On the theoretical front, many attempts were proposed for predicting the electron-induced ionization of simple biological molecules including DNA/RNA components. However, these latter are - in the major part - restricted to semi-empirical approaches like that proposed by Deutsch and Märk [13] usually referred as DM model and the well-known binary encounter dipole (BED) and binary encounter Bethe (BEB) models reported by Kim and Rudd [14]. In this context, a quantum-mechanical model has been recently proposed by Champion [15] for describing the electron-induced ionization process on DNA with in particular an extensive theory/experiment comparison in terms of *total* ionization cross sections for DNA bases and THF molecule. From this point of view, the current work may be seen as an extension of this previous work to the multi-differential scale. Thus, to the best of our knowledge, the present study appears

as the first comparison between theoretical predictions and experimental data in terms of *angular* and *energetic* distributions for secondary electrons produced by electron impact on THF isolated molecules. Besides a theory/experiment comparison, we will also report here a detailed discussion on the influence of the ejected electron modeling as well as that of the impacted target on the multiple differential cross sections. In this context, two descriptions of the THF electronic ground-state, using the restricted Hartree-Fock (RHF) method with different Gaussian-type basis sets, namely, the RHF/3-21G and the RHF/6-311G levels of theory will be studied.

2. Theoretical approach

In the sequel, the theory will be briefly reported and for more details we refer the reader to the above-cited previous work [15].

Let us first remind that the doubly differential cross sections (DDCS) reported here are calculated within the 1st Born approximation framework by using the partial-wave expansion formalism recently employed by Champion for describing the ionization process induced by electron impact on isolated DNA components including both the nucleobases and the sugar phosphate backbone [15].

In this context, the electron-induced ionization process of a molecular target like that here studied will be assumed to be reduced to a one-active electron problem by considering the passive (not ionized) electrons as frozen in their molecular orbitals during the collision. Thus, the interaction potential $V(\boldsymbol{r}_0,\boldsymbol{r}_1)$ between the incident electron and the target may be simply written as

$$V(\boldsymbol{r}_0,\boldsymbol{r}_1)=\frac{1}{|\boldsymbol{r}_0-\boldsymbol{r}_1|}-\frac{1}{r_0}, \qquad (1)$$

where with $\boldsymbol{r}_0$ and $\boldsymbol{r}_1$ stand for the position vectors of the incident and the active target electron, respectively.

Besides, let us note remind that the molecular triply differential cross sections are expressed as a weighted sum of “atomic orbital” triply differential cross sections corresponding to the different atomic components involved in the current description of the molecular target here investigated, namely, within a complete neglected differential overlap (CNDO) approach. Electronic structure calculations for THF were carried out in the gas phase using the Gaussian 09 ab initio quantum chemistry software package [16], without symmetry constraints imposed during geometry optimization. As stated above, the THF electronic ground-state was described using the restricted Hartree-Fock (RHF) method with two different split-valence Gaussian basis sets, namely, the 3-21G double-zeta and 6-311G triple-zeta basis sets implemented in Gaussian 09. Bernhardt and Paretzke [17] previously found that the molecular parameters calculated at the RHF/3-21G level were in good agreement with the experiments for DNA-type components. Moreover, we observed that the application of larger basis sets - including diffuse and polarization functions, for geometric optimization and single-point calculation - generally led to larger overestimations of the ionization potentials, for example. Thus, only minute discrepancies were found here in terms of bond distances and angles calculated within the RHF/3-21G and RHF/6-311G approaches. Finally, the experimental value of 9.45 eV for the first ionization potential of THF [18] was inserted in the calculations, instead of the computed values, to fix the threshold behavior of the ionization cross section at the experimental value. The input parameters needed for the THF description, namely, the binding energy (B) as well as the atomic population for each molecular orbital are reported hereafter in Table 1. As can be seen, the different theoretical descriptions at the RHF/3-21G and RHF/6-311G levels result only in relatively small differences in binding energies and populations.

Molecular orbitals	*B*(eV) RHF/3-21G	*B*(eV) RHF/6-311G	Population RHF/3-21G	Population RHF/6-311G
1	9.45	9.45	0.48 H(1s) + 0.24 C(2p) + 1.26 O(2p)	0.48 H(1s) + 0.28 C(2p) + 1.26 O(2p)
2	10.616	10.637	0.04 H(1s) + 0.92 C(2p) + 0.08 O(2s) + 0.92 O(2p)	0.04 H(1s) + 0.96 C(2p) + 0.06 O(2s) + 0.88 O(2p)
3	11.378	11.149	0.84 H(1s) + 1.12 C(2p)	0.96 H(1s) + 1.04 C(2p)
4	11.579	11.661	0.44 H(1s) + 1.52 C(2p)	0.50 H(1s) + 1.50 C(2p)
5	11.83	11.684	0.36 H(1s) + 1.28 C(2p) + 0.28 O(2p)	0.34 H(1s) + 1.28 C(2p) + 0.30 O(2p)
6	13.901	12.988	0.44 H(1s) + 0.84 C(2p) + 0.70 O(2p)	0.48 H(1s) + 0.84 C(2p) + 0.64 O(2p)
7	13.901	13.709	0.40 H(1s) + 0.96 C(2p) + 0.54 O(2p)	0.44 H(1s) + 0.96 C(2p) + 0.60 O(2p)
8	14.211	13.942	0.72 H(1s) + 1.24 C(2p)	0.76 H(1s) + 1.24 C(2p)
9	15.829	15.618	0.36 H(1s) + 1.20 C(2p) + 0.06 O(2s) + 0.34 O(2p)	0.36 H(1s) + 1.16 C(2p) + 0.04 O(2s) + 0.38 O(2p)
10	16.305	16.014	0.52 H(1s) + 1.16 C(2p) + 0.28 O(2p)	0.52 H(1s) + 1.16 C(2p) + 0.32 O(2p)
11	19.281	18.993	0.44 H(1s) + 1.04 C(2s) + 0.28 C(2p) + 0.16 O(2p)	0.52 H(1s) + 1.02 C(2s) + 0.28 C(2p) + 0.18 O(2p)
12	19.424	19.063	0.44 H(1s) + 1.02 C(2s) + 0.36 C(2p) + 0.14 O(2s)	0.48 H(1s) + 1.00 C(2s) + 0.36 C(2p) + 0.12 O(2s)
13	23.637	23.346	0.20 H(1s) + 1.60 C(2s) + 0.14 O(2p)	0.20 H(1s) + 1.52 C(2s) + 0.16 O(2p)
14	25.279	24.812	0.16 H(1s) + 1.56 C(2s) + 0.08 C(2p) + 0.18 O(2s)	0.16 H(1s) + 1.52 C(2s) + 0.08 C(2p) + 0.18 O(2s)
15	32.111	31.725	0.40 C(2s) + 0.04 C(2p) + 1.46 O(2s) + 0.08 O(2p)	0.32 C(2s) + 0.04 C(2p) + 1.52 O(2s) + 0.08 O(2p)
16	265.909	261.458	1.98 C(1s)	2.00 C(1s)
17	265.933	261.458	1.98 C(1s)	2.00 C(1s)
18	266.909	262.412	2.00 C(1s)	2.00 C(1s)
19	266.909	262.412	2.00 C(1s)	2.00 C(1s)
20	486.377	477.994	2 .00 O(1s)	2.00 O(1s)

Table 1: RHF/3-21G and RHF/6-311G descriptions of the tetrahydrofuran molecule.

Thus, in the laboratory framework, the 1st Born triply differential cross sections, namely differential in the direction of the scattered projectile Ω_s, differential in the direction of the ejected electron Ω_e and differential in the ejected energy E_e, hereafter denoted $\sigma^{(3)}(\Omega_s,\Omega_e,E_e)=\dfrac{d^3\sigma}{dE_e d\Omega_e d\Omega_s}$, may be expressed as

$$\sigma^{(3)}(\Omega_s,\Omega_e,E_e)=(2\pi)^4.\frac{k_s k_e}{k_i}.\sum_{j=1}^{N}\sum_{i=1}^{N_{at}(j)}\xi_{j,i}.\left|\left[T_{a,b}\right]_i\right|^2, \tag{2}$$

where $\left[T_{a,b}\right]_i$ denotes the transition matrix element between an initial state *a* and a final state *b* and is expressed by

$$\left[T_{a,b}\right]_i=\left\langle\varphi_b^i(\boldsymbol{r}_1).\phi_b^i(\boldsymbol{r}_0)\middle|V(\boldsymbol{r_0},\boldsymbol{r_1})\middle|\varphi_a^i(\boldsymbol{r}_1).\phi_a^i(\boldsymbol{r}_0)\right\rangle. \tag{3}$$

In Eq.(2), *N* represents the number of molecular orbitals used in the THF target description ($N = 20$) while $\xi_{j,i}$ refers to the effective number of electrons in the *i*-th atomic component of the *j*-th molecular orbital of the ionized target. Besides, in Eq.(3) $\phi_a^i(\boldsymbol{r_0})$ and $\phi_b^i(\boldsymbol{r_0})$ refer to the incident and the scattered projectile, respectively - both described by a plane wave - whereas $\varphi_a^i(\boldsymbol{r_1})$ stands for the atomic wave function of the i^{th}-orbital (with *i* ranging from 1 to $N_{at}(j)$) used in the CNDO expansion of each of the *N* target molecular subshells. The atomic wave functions are here expanded on spherical harmonic basis with a radial part given in terms of Slater functions, namely,

$$\varphi_a^i(\boldsymbol{r})=\sum_{k=1}^{N_i}\frac{(2\varsigma_k)^{n_{ik}+1/2}}{\sqrt{(2n_{ik})!}}.r^{n_{ik}-1}.e^{-\varsigma_{ik}.r}.Y_{l_{ik}m_{ik}}(\Omega_r)\equiv\sum_{k=1}^{N_i}f_{ik}(r).Y_{l_{ik}m_{ik}}(\Omega_r), \tag{4}$$

where N_i denotes the number of partial waves (n_{ik},l_{ik},m_{ik}) used for the description of the i^{th} atomic orbital (for more details about these coefficients, see the Clementi's tables of atomic functions [19] and details about their use in Ref.[20]).

Additionally, in Eq.(3) $\varphi_b^i(\boldsymbol{r_1})$ represents the ejected-electron Coulomb wave function,

whose Sommerfeld parameter - defined as the ratio between the product of the charges of the particles and their relative momentum - is equal to Z_e/k_e where Z_e corresponds to the effective ionic charge seen by the escaping electron. In the current work, the latter will be considered either as a constant value ($Z_e = 1$ or $Z_e = Z_T^*$, see hereafter) or dynamical ($Z_e = Z_d$) and then dependent of the kinematics of the collision via the relation reported in our previous work [21], namely

$$Z_d = 1 - \frac{2k_{s1}k_1^2}{(k_s + k_1)^3}\left(\frac{3+\cos^2(4\varepsilon(k_s))}{4}\right)^2 \quad \text{with} \quad \begin{cases} k_{s1} = \frac{1}{2}\left|\boldsymbol{k_s} - \boldsymbol{k_1}\right| \\ \varepsilon(k_s) = \arccos\left(\frac{k_s}{\sqrt{k_s^2 + k_1^2}}\right). \end{cases} \tag{5}$$

In fact, in the first (constant) case, we will distinguish the asymptotic target charge from the effective one, namely, $Z_e = 1$ and $Z_e = Z_T^* = \sqrt{2n^2B}$, respectively, where n refers to the principal quantum number of each atomic orbital component used in the molecular target description.

Finally, let us add that in Eqs.(2) and (5) $\boldsymbol{k_i}$, $\boldsymbol{k_s}$, and $\boldsymbol{k_e}$ represent the wave vectors of the incident, the scattered and the ejected electron, respectively, while $\boldsymbol{q} = \boldsymbol{k_i} - \boldsymbol{k_s}$ denotes the momentum transfer.

Thus, within the partial-wave expansion formalism, Eq.(2) may be reduced to

$$\sigma^{(3)}(\Omega_s, \Omega_e, E_e) = \frac{32k_s}{k_i k_1 q^4}\sum_{j=1}^{N}\sum_{i=1}^{N_{at}(i)}\left\{\left(\frac{X'_{ij}(k_1)}{4\pi}\right)^2 + \sum_{\mu=-l_{ij}}^{l_{ij}}\left[\left|Z_{ij}(k_1,q)\right|^2 - \Re e\left(\frac{Z_{ij}}{\sqrt{\pi\hat{l}_{ij}}}Y^*_{l_{ij}\mu}\left(\Omega_{k_1}\right)i^{l_{ij}}e^{-i\sigma_{l_{ij}}}X'_{ij}(k_1)\right)\right]\right\} \tag{6}$$

where $\Re e(z)$ denotes the real part of the complex z and

$$\begin{cases} X_{ij}^{'}(k_1) = \int_0^\infty dr.r.F_{l_{ij}}(k_1,r).f_{ij}(r) \\ Z_{ij}(k_1,q) = \sum_{l=0}^{\infty} \sum_{l_1=|l-l_{ij}|}^{l+l_{ij}} \sum_{m_1=-l_1}^{l_1} i^{l-l_1} e^{i\sigma_{l_1}} X_{ij}^{ll_1}\ Y_{l_1 m_1}(\Omega_{k_1})\, Y_{lm_1-\mu}^{*}(\Omega_q)\,(-1)^{m_1} \sqrt{\hat{l}_1 \hat{l}} \begin{pmatrix} l_1 & l & l_{ij} \\ 0 & 0 & 0 \end{pmatrix} \begin{pmatrix} l_1 & l & l_{ij} \\ -m_1 & m_1-\mu & \mu \end{pmatrix}, \end{cases} \quad (7)$$

with

$X_{ij}^{ll_1}(k_1,q) = \int_0^\infty dr.r.F_{l_1}(k_1,r).j_l(qr).f_{ij}(r)$ and $\hat{l} = 2l+1$.

Let us note that, in Eq.(6) σ_l refers to the Coulomb phase shift, while in Eq.(7) $F_{l_1}(k_1,r_1)$ denotes the radial hypergeometric function solution and $j_l(qr)$ the Bessel function (see Ref.**[**20] for more details).

Doubly differential ionization cross sections were then finally obtained from Eq.(6) after numerical integration of the triply differential cross sections over the scattering direction while singly differential and then total cross sections (SDCS and TCS, respectively) were deduced from integration over the ejection direction and the energy transfer, respectively.

3. Experimental method

Absolute doubly differential inelastic cross sections of THF were determined for electron energies ranging from 20 eV to 1 keV at the Physikalisch Technische Bundesanstalt (PTB, Braunschweig, Germany) using a crossed-beam arrangement. Details on this experiment will be published elsewhere while the principle has been described by Baek et al. [8] for the differential elastic scattering cross sections of THF. In brief, a collimated beam of mono-energetic electrons with a current between 1 pA and 1 nA perpendicularly crosses a molecular beam. The density of the molecular beam is chosen low enough to fulfill single scattering conditions. The count rate of electrons scattered into a solid angle segment was measured as function of the energy of the scattered electrons. This was achieved by placing the detector system at different angles between 15° and 135° relative to the direction of the incident particles. The energy of the scattered electrons was selected between 2.7 eV and the primary electron energy by a hemispherical mirror analyzer (HMA). The measured count rate of scattered electrons is proportional to the DDCS and

can be appointed to the absolute scale by characterizing the HMA detection efficiency and number density per area of molecules in the interaction volume. The latter is obtained by measuring the reduction of the electron beam current in forward direction and by using the total scattering cross sections that were measured by an independent linear transmission experiment [8].

4. Results and discussion

We report in Figure 1, the theoretical doubly differential cross sections for ionization of a THF molecule described within the RHF/3-21G level of theory for an incident electron energy E_i = 100 eV and for a selection of ejection energies *i.e.* E_e = 10.1 eV, E_e = 20.1 eV, E_e = 30.1 eV, E_e = 40.1 eV, and E_e = 50.1 eV. The three models of effective ionic charge seen by the escaping electron as reported above are shown, namely, the asymptotic charge $Z_e = 1$ (solid line), the effective target charge $Z_e = Z_T^*$ (dashed line) and finally the dynamical charge $Z_e = Z_d$ (dotted line). It clearly appears a strong influence of the latter on the DDCS calculations, in particular when $Z_e = Z_T^*$. In effect, in comparison to the asymptotic charge case, the use of the effective charge tends to diminish the amplitude of the DDCS over the whole range of ejection angles, with nevertheless a stronger influence when the ejected electron is slow (here E_e = 10. eV), what points out that the attractive interaction between the ejected electron and the ionized target is all the more important as the secondary electron is slow. Regarding now the use of the dynamical charge Z_d (dotted line), no difference is visible except in the backward direction ($\theta_e > 90°$) especially when the ejected electron energy increases (here E_e = 50.1 eV).

In comparison to the experimental measurements, the theoretical data generally overestimate the DDCS at forward scattering angles, while those in backward direction are slightly underestimated. Apart from the discrepancies on the absolute scale, the trend of the experimental DDCS as function of the ejection energy E_e is well reproduced by the theory. Thus,

we obviously observe that for low energies E_e the ejection is more isotropic while a pronounced peak is formed and shifts towards the binary peak at forward scattering angles with increasing E_e.

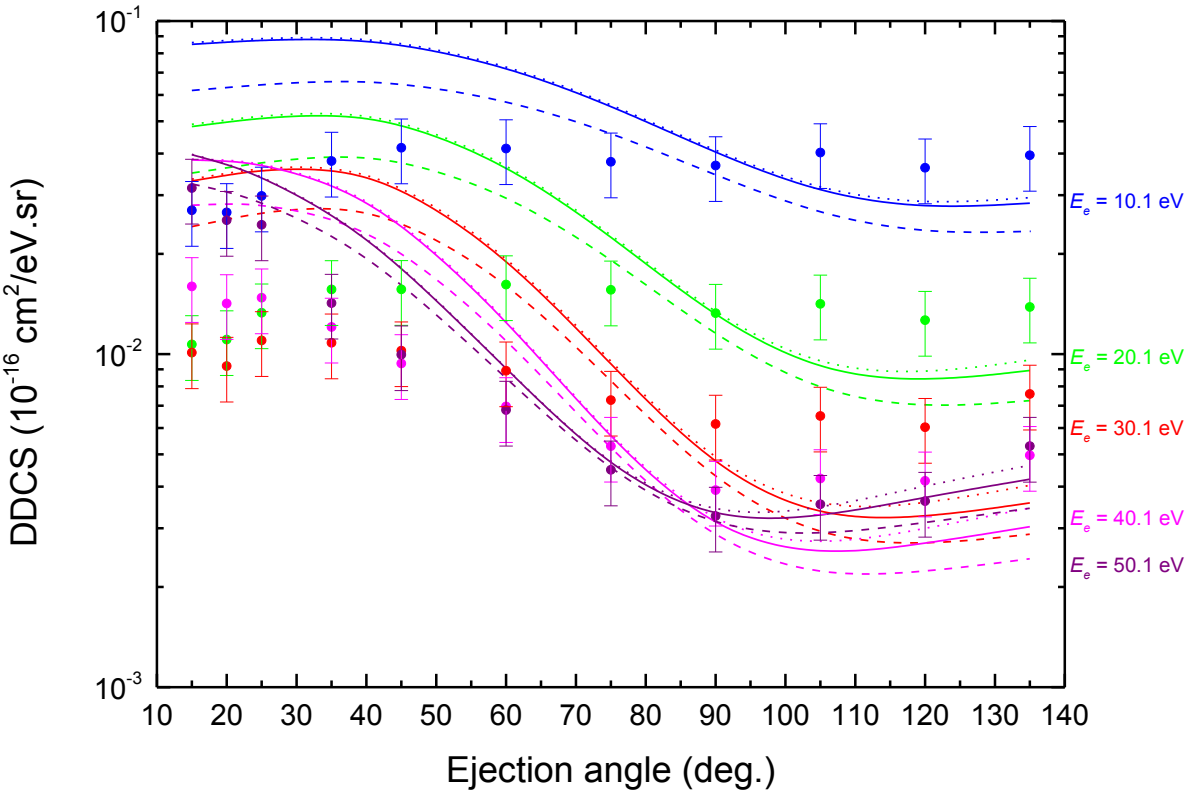

Figure 1: (Color online) Doubly differential cross sections of THF electron-induced ionization for an incident energy $E_i = 100$ eV and for selected ejected energies E_e. Comparison between experimental measurements (symbols) and theoretical predictions ($Z_e = 1$: solid line, $Z_e = Z_T^*$: dashed line and $Z_e = Z_d$: dotted line). The THF molecule is here described within the RHF/3-21G level of theory.

Similar calculations were also performed with a THF molecule described within the RHF/6-311G level of theory. The corresponding results are shown in Figure 2. No evident

difference appear with the results reported in Figure 1, what clearly points out that the level of target description is not so important, even considering the differential scale for describing the ionization process.

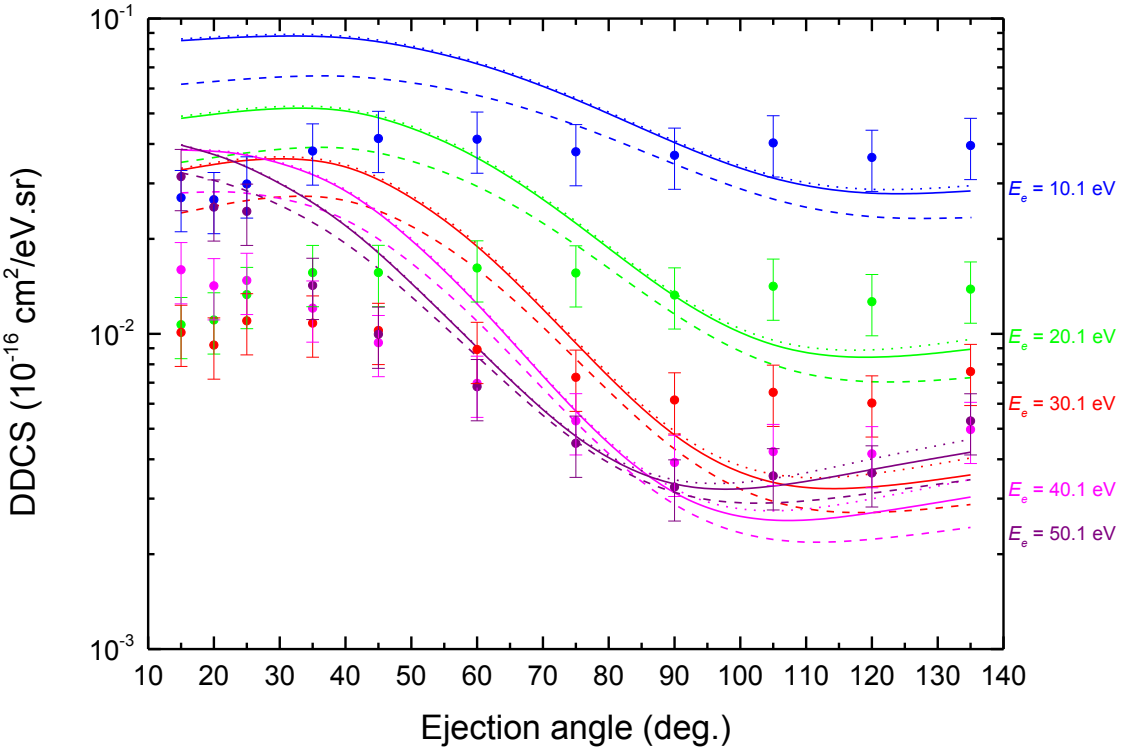

Figure 2: (Color online) Same as in Figure 1 with a THF molecule described within the RHF/6-311G level of theory.

In a second step, the doubly differential cross sections were numerically integrated so as to provide singly differential cross sections (SDCS), which are reported in Figure 3 (for a THF molecule described within the RHF/3-21G level of theory) and compared to the experimental measurements. Thus, consequently to the overestimation of the DDCS above reported - in particular in the forward direction ($\theta_e < 90°$) - the SDCS also obtained exhibit here a disagreement of the order of 30% over the whole range of ejection energies, the latter being more

pronounced for the asymptotic charge and the dynamical charge model since the SDCS obtained with $Z_e = Z_T^*$ exhibit a good agreement with the experiment.

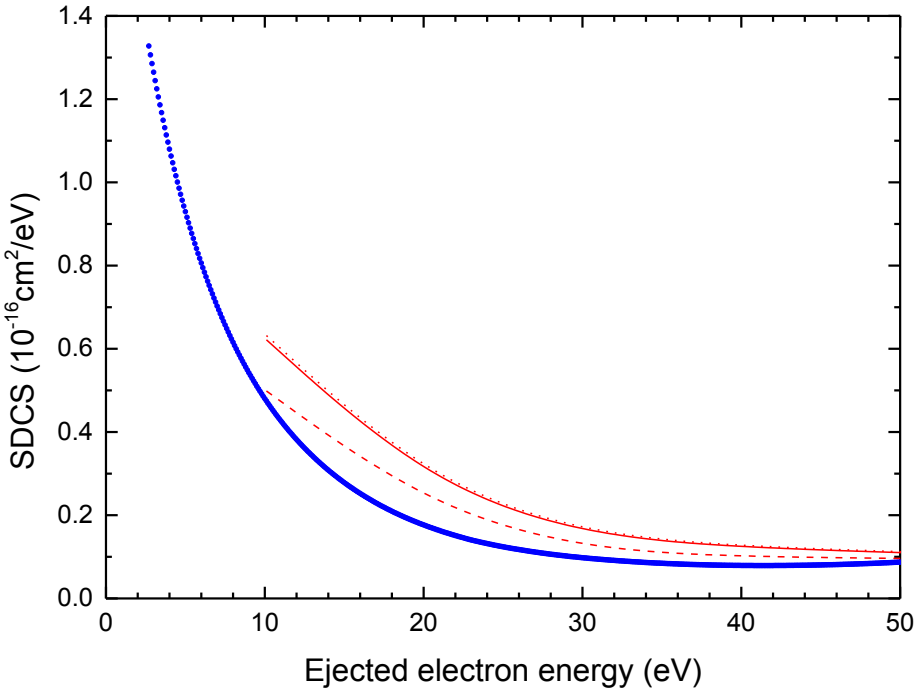

Figure 3: (Color online) Singly differential cross sections of THF electron-induced ionization for an incident energy E_i = 100 eV Comparison between experimental measurements (symbols) and theoretical predictions ($Z_e = 1$: solid line, $Z_e = Z_T^*$: dashed line and $Z_e = Z_d$: dotted line). The THF molecule is here described within the RHF/3-21G level of theory.

Finally, by integration of the SDCS over the ejection energy range (from ≅ 0 eV to E_i/2), we obtained the total ionization cross sections reported in Table 2. The best agreement with the experimental value is obtained when using the effective charge description in the theoretical approach. However, a comparison to the ionization cross section of (12,5 ± 0,9).10^{-16} cm^2, determined by Fuss et al. [5], indicates that these theoretical data overestimate the total ionization cross section by 20-40% with respect to the experimental data. Similarly, the current theoretical

TCS value appears as greater than the BEB semi-empirical prediction of 12,43.10^{-16}cm2 reported by Możejko and Sanche [22].

	$Z_e = 1$ model	$Z_e = Z_T^*$ model	$Z_e = Z_d$ model	Experimental
σ_{100eV} (10^{-16} cm^2)	21,98	17,95	22,54	15 ± 3

Table 2: Comparison between the different theoretical predictions and experiment in terms of total cross sections of THF electron-induced ionization for an incident energy E_i = 100 eV. The THF molecule is here described within the RHF/3-21G level of theory

5. Conclusions

We have investigated in this work a detailed theoretical approach to describe the electron-induced ionization of isolated tetrahydrofuran molecules. Doubly and singly differential cross sections were then successively compared to recent experimental data. From a general point of view and even considering that the overall behavior of the DDCS was well reproduced, we clearly pointed out an overestimation of the experimental DDCS at forward scattering angles and a less pronounced underestimation in the backward direction, that nevertheless tends to disappear when the ejection energy increases. Additionally, we have shown that the description of the ejected electron may have a crucial importance in the cross section calculation while the influence of the target modeling was found as minor.

In this context, it clearly appears that theoretical developments are still required in order to accurately model the electron-impact ionization process for complex target molecules such as biomolecules. Thus, future theoretical work on this problem will be directed at incorporating distorted waves into all channels of the process.

Acknowledgments

This work has been developed as part of the activities planned in the project PICS 5921 (THEOS) of the Centre National de la Recherche Scientifique. Besides, C. C. and M. A. Q. would like to thank P. Senot (Univ. Lorraine) for his kind assistance in the numerical developments and for the free computer time provided. The experimental work was carried out within EMRP Joint Research Project SIB06 BioQuaRT. The EMRP is jointly funded by the EMRP participating countries within EURAMET and the European Union. Sandia National Laboratories is a multi-program laboratory managed and operated by Sandia Corporation, a wholly owned subsidiary of Lockheed Martin Corporation, for the U.S. Department of Energy's National Nuclear Security Administration under contract DE-AC04-94AL85000.

References

[1] F. Blanco and G. Garcia, Physics Letters A **360**, 707-712 (2007)

[2] C. J. Colyer, S. M. Bellm, B. Lohmann, G. F. Hanne, O. Al-Hagan, D. H. Madison, and C. G. Ning, J. Chem. Phys. **133**, 124302 (2010)

[3] J. D. Builth-Williams, S. M. Bellm, D. B. Jones, H. Chaluvadi, D. H. Madison, C. G. Ning, B. Lohmann, and M. J. Brunger, J. Chem. Phys. **136**, 024304 (2012)

[4] S. M. Bellm, C. J. Colyer, B. Lohmann, and C. Champion, Phys. Rev. A **85**, 022710 (2012)

[5] M. Fuss, A. Muñoz, J. C. Oller, F. Blanco, D. Almeida, P. Limao Vieira, T. P. D. Do, M. J. Brunger, and G. García, Phys. Rev. A **80**, 052709 (2006)

[6] M. Dampc, E. Szymańska, B. Mielewska, and M. Zubek, J. Phys. B **44**, 055206 (2011)

[7] P. Możejko, E. Ptasińska-Denga, A. Domaracka, and C. Szmytkowski, Phys. Rev. A **74**, 012708 (2006)

[8] W.Y. Baek, M. Bug, H. Rabus, E. Gargioni, and B. Grosswendt, Phys. Rev. A **86**, 032702 (2012)

[9] M. I. Shafranyosh, M. I. Sukhoviya, L. L. Shimon, and I. I. Shafranyosh, Technical Physics Letters **31(12)**, 1071-1073 (2005),

[10] I. I. Shafranyosh, M. I. Sukhoviya, and M. I. Shafranyosh, J. Phys. B: At. Mol.Opt. Phys. **39**, 4155-4162 (2006)

[11] I. I. Shafranyosh, M. I. Sukhoviya, M. I. Shafranyosh, and L. L. Shimon, Technical Physics **53(12)**, 1536-1540 (2008)

[12] S. Feil, K. Gluch, S. Matt-Leubner, P. Scheier, J. Limtrakul, M. Probst, H. Deutsch, K. Becker, A. Stamatovic, and T. D. Märk, J. Phys. B: At. Mol. Opt. Phys. **37**, 3013-3020 (2004)

[13] H. Deutsch and T. D. Märk, Int. J. Mass Spectrom. Ion Process. **79**, R1 (1987)

[14] Y. K. Kim and M. E. Rudd, Phys. Rev. A **50**, 3954 (1994)

[15] C. Champion, J. Chem. Phys. **138**, 184306 (2013)

[16] M. J. Frisch et al, Gaussian 09, Revision A.02, Gaussian, Inc., Wallingford CT (2009)

[17] P. Bernhardt and H. G. Paretzke, Int. J. Mass Spectrom **599**, 223–224 (2003)

[18] http://www.indsci.com/docs/manuals/VX500_IP.pdf

[19] E. Clementi and R. Roetti, Atomic Data and Nuclear Data Tables **14**,177–478 (1974)

[20] C. Champion, J. Hanssen, and P. -A. Hervieux, J. Chem. Phys. **117**, 197-204 (2002)

[21] C. Champion, C. Dal Cappello, S. Houamer, and A. Mansouri, Phys. Rev. A. **73**, 012717 (2006)

[22] P. Możejko and L. Sanche, Radiat. Phys. Chem. **73**, 77-84 (2005)